Synthesis of two-dimensional single-crystal berzelianite nanosheets and nanoplates with near-infrared optical absorption†

Zhengtao Deng,*[ab] Masud Mansuripur[b] and Anthony J. Muscat[a]

Received 14th April 2009, Accepted 8th June 2009
First published as an Advance Article on the web 6th July 2009
DOI: 10.1039/b907452j

The solar cell industry requires convenient and inexpensive fabrication of semiconductor nanostructures as highly efficient absorptive layers with low-cost, environmentally benign, heavy-metal-free (*i.e.*, free from Hg, Cd, and Pb) and suitable band gap near 1 eV features. In this paper, we demonstrate the synthesis of two-dimensional single-crystal berzelianite ($Cu_{2-x}Se$) nanosheets (in-plane diameter-to-thickness ratio ~100) and nanoplates (in-plane diameter-to-thickness ratio ~10) *via* a simple, "green" and environmentally benign method of injecting Cu(I)-complex precursor into Se-solution in paraffin liquid. Unlike the previous syntheses of binary chalcogenide nanostructures such as CdSe, the current strategy for berzelianite synthesis does not use expensive and toxic phosphine ligands such as trioctylphosphine (TOP). The products were characterized by a range of methods, such as X-ray powder diffraction, scanning electron microscopy, energy-dispersive X-ray spectroscopy, transmission electron microscopy, and selected area electron diffraction, revealing that the products have the cubic phase and high-quality single-crystal two-dimensional nanostructure. UV-Vis-NIR absorption spectroscopy reveals that the nanosheets and nanoplates show obvious absorption onsets at 0.89 eV and 0.80 eV, respectively, and strong optical absorption peak at 1.70 eV and 1.62 eV, covering the whole red range of the solar spectrum. The present study opens a new avenue to "green" and low-cost controllable synthesis of binary chalcogenides with technological applications in solar energy conversion and also in a wide range of photonic devices operating in the near-infrared.

1. Introduction

Semiconductor nanostructures are promising building blocks for future-generation solar cells due to their high absorption coefficients, controllable band gaps, and radiation stability.[1–3] All of these could offer processing, scale, and cost advantages when compared with conventional single crystal and thin-film solar cells. One of the main challenges in this area is to fabricate high-quality, nanostructured, semiconducting materials using low-cost, earth-abundant, environmentally-benign, and heavy-metal-free (*i.e.*, free from Hg, Pb, and Cd) compounds with a suitable maximum in the E_g range of 0.8–1.4 eV.[4–6]

Transition-metal binary chalcogenide nanostructures have been extensively investigated for their potential applications to photovoltaic and photonic devices.[7,8] Among them, copper sulfide and copper selenide are semiconductors with p-type conductivity and band gaps near 1 eV.[9] This class of materials could be used for solar energy conversion as a highly efficient absorber layer material, and also in a number of other industrial applications including infrared detection and imaging; their use as pigments has also been investigated.[10,11] Copper selenide has received attention due to its particular photoelectric properties and wide applications in electronic and optoelectronic devices, such as solar cells, optical filters, super ionic conductors, photodetectors, and Schottky-diodes.[12,13] The copper selenide group comprises various compounds such as cubic berzelianite (Cu_2Se, $Cu_{1.8}Se$, $Cu_{2-x}Se$), tetragonal umangite (Cu_3Se_2), hexagonal klockmannite (CuSe, $Cu_{0.87}Se$), and orthorhombic athabascaite (Cu_5Se_4, CuSe).[14–17] All of these phases have been identified as p-type semiconducting materials because of the copper vacancies within the lattice.[18,19]

Recently, great progress has been made in the synthesis of Cu_2S nanocrystals for application in solar cells. In 2007, Park *et al.*[20] reported the synthesis of Cu_2S nanocrystals on multi-walled carbon nanotubes and demonstrated their application in solar cells; the power conversion efficiency of this structure, however, was only about 0.08%. In 2008, Alivisatos *et al.*[21] reported the synthesis of colloidal Cu_2S nanocrystals and demonstrated their application as an active light-absorbing component in combination with CdS nanorods to make a solution-processed solar cell with 1.6% power conversion efficiency with stability over a four-month testing period. In contrast, less progress has been made for its counterpart, copper selenide, for solar cells application, possibly due to the challenges to obtaining high-quality copper selenide nanostructures using a simple, inexpensive, and "green" approach. In the past few years, there have been only a few reports of copper selenide nanostructure synthesis.[22–27] For example, O'Brien *et al.*[22] reported a single-source route to synthesise CuSe nanoparticles by thermolysis of $Cu(Se_2CNEt_2)_2$ in trioctylphosphine oxide (TOPO). Cao *et al.*[26]

[a]*Department of Chemical and Environmental Engineering, The University of Arizona, Tucson, Arizona, 85721, USA. E-mail: dengz@email.arizona.edu*
[b]*College of Optical Sciences, The University of Arizona, Tucson, Arizona, 85721, USA*

† Electronic supplementary information (ESI) available: Additional SEM and TEM images, size distribution histograms of the nanosheets and nanoplates. See DOI: 10.1039/b907452j

reported the synthesis of Cu_3Se_2 nanoplates through a microwave-enhanced reaction. Nevertheless, synthesis of high-quality single-crystal copper selenide nanostructures (with potential applications in solar energy conversion) continues to pose difficulties. To our knowledge, there has been no report demonstrating the controllable synthesis of two-dimensional copper selenide nanostructures.

In this paper, we report the first synthesis of two-dimensional, single-crystal nanosheets (in-plane diameter-to-thickness ratio ~100) and nanoplates (in-plane diameter-to-thickness ratio ~10) of berzelianite ($Cu_{2-x}Se$) in a "green" and low-cost organic solvent (paraffin liquid), together with 2-ethylhexanoic acid (EHA) and oleylamine (OAm) as simple and low-cost ligands, without use of expensive and toxic phosphine ligands such as trioctylphosphine (TOP). UV-Vis-NIR absorption spectroscopy reveals that the nanosheets and nanoplates have strong absorption bands covering the entire red range of the solar spectrum.

2. Experimental

All of the chemical reagents used in the experiments were purchased from Sigma-Aldrich. In a typical synthesis of berzelianite nanosheets, first, Cu(I)-complex precursor solution was prepared by adding 0.50 mmol of copper (I) chloride (CuCl, ≥99.8%) to 2 mL 2-ethylhexanoic acid (EHA, 99+%) and 2 mL oleylamine (OAm, technical grade, 70%) in a flask and kept at 80 °C and stirred for 30 minutes until a uniform mixture was formed, then cooled to room temperature. Second, selenium-precursor solution was prepared in a separate flask, where 0.25 mmol of bulk Se powder was mixed with 20 mL paraffin liquid and kept at 250 °C, then stirred for 30 minutes. Third, Cu(I)-complex precursor solution was swiftly injected into the selenium-precursor solution and maintained at 250 °C. Immediately after injection, the color of the mixed solution turned from light yellow to dark, indicating the formation of the $Cu_{2-x}Se$ species. The reaction could be performed under N_2 gas or open to air. Serial aliquots (2 mL) were taken for monitoring the kinetics of product formation. After 10 minutes, hexane and isopropyl alcohol (IPA) were added, and the resulting solid products were retrieved by centrifugation. The final products were dispersible in many organic solvents such as IPA, toluene and hexane. The synthesis of the nanoplates is similar to nanosheets except using 0.25 mmol CuCl, instead of 0.50 mmol.

X-ray powder diffraction (XRD) measurements employed a Philips X-ray diffractometer (PW3710, The Netherlands) with Cu Kα radiation (λ = 1.5418 Å) and scanned at a rate of 2 deg/min. Scanning electron microscopy (SEM) and energy-dispersive X-ray spectroscopy (EDS) were preformed on a Hitachi S-4800 scanning electron field emission microscope and a Hitachi S-3400N scanning electron field emission microscope. TEM images were obtained either using a JEOL JEM 100X TEM with a 100-kV accelerating voltage or a Hitachi H8100 electron microscope operating at 200 kV. Ultraviolet-Visible-Near Infrared (UV-Vis-NIR) absorption spectra were recorded at room temperature with a JASCO V-670 spectrophotometer equipped with an integrating sphere (Model: ISN-723, diameter: 60 mm). Samples for XRD and UV-Vis-NIR) absorption characterizations were prepared by drop coating of concentrated nanosheet and nanoplate samples in hexane onto a clean glass substrate.

3. Results and discussion

As shown in Fig. 1, our synthesis of cubic berzelianite nanosheets and nanoplates involves the injection of Cu(I)-complex precursor into a hot (250 °C) paraffin liquid containing bulk Se powder. The chemical reactions involved in the formation of the $Cu_{2-x}Se$ nanosheets and nanoplates are supposed to be similar to those reported in the literature for the synthesis of CdSe nanocrystals, which do not need the expensive and toxic phosphine ligands such as trioctylphosphine (TOP), and are thus expected to be a "greener" and lower-cost technique.[28–30] In a detailed growth process, under heating, the Se powder is reduced to H_2Se, while the long alkane chain is oxidated to long alkene chain; at the same time, CuCl reacts with the EHA and OAm to form Cu(I)-complex; subsequently, Cu(I)-complex reacts with H_2Se to form $Cu_{2-x}Se$ nanosheets and nanoplates.

Our XRD studies confirmed that the nanosheets and nanoplates prepared with our method are both cubic berzelianite. As shown in Fig. 2, the experimental XRD profiles taken from the samples reveal that all of the peaks are close to the standard profile for cubic berzelianite (cell constants $a = 5.739$ Å; JCPDS Card No. 06–0680). No peaks of bulk Se powder or any other phases were detected, indicating that the products are single-phase samples of high-purity. In addition, the intense and sharp diffraction peaks suggest that the as-synthesized products are well-crystallized.

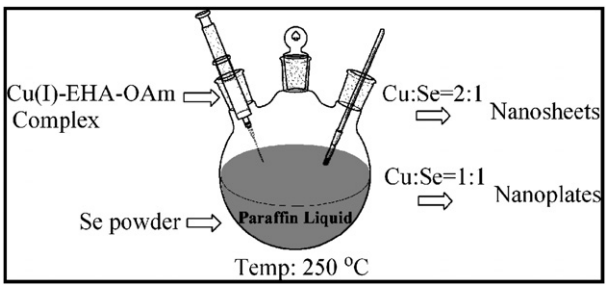

Fig. 1 Schematic diagram illustrating the synthesis of single-crystal $Cu_{2-x}Se$ nanosheets and nanoplates. EHA: 2-Ethylhexanoic acid, $CH_3(CH_2)_3CH(C_2H_5)COOH$; OAm: oleylamine $CH_3(CH_2)_7CH{=}CH(CH_2)_7CH_2NH_2$; Paraffin liquid: $CH_3(CH_2)_nCH_3$, (n = 16–22).

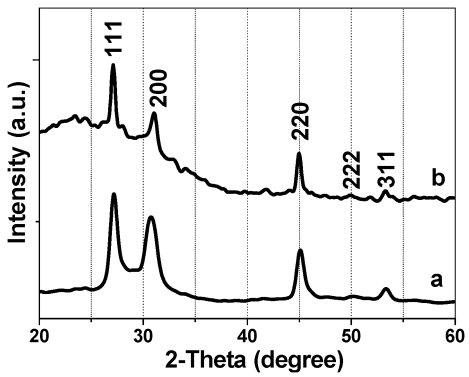

Fig. 2 XRD patterns of the berzelianite (a) nanosheets and (b) nanoplates.

The morphology and size of the berzelianite nanosheets (in-plane diameter-to-thickness ratio ~100) were studied in detail using SEM. Fig. 3a and Figure S1 (see ESI†) show that the product contains a large quantity of ulthathin sheet-like materials. Figs. 3b-3d show the high magnification SEM image of nanosheets indicating that the size, thickness, and morphology of the product are quite uniform. Figs. 3c-3d demonstrate several typical regular-shaped (triangular, truncated triangular, and hexagonal) nanosheets with their basal plane parallel to the silicon substrate, indicating that the in-plane diameters of the products are between 1.0–2.5 μm. The thickness of the nanosheets was estimated from the closer SEM image. Figs. 3e-3f show typical nanosheets with their basal plane upright to the silicon substrate, revealing that these micron-scale nanosheets have the ultrathin thickness of 12 and 16 nm, respectively. As revealed by the distribution histograms (see ESI†), the in-plane diameter-to-thickness ratio is estimated to be ~100. Fig. 3g is an EDS spectrum obtained from the nanosheets shown in the inset. Only Cu and Se peaks are observed (the silicon signal is from the substrate), suggesting that these nanoplates are composed mainly of Cu and Se. Quantitative EDS analysis shows that the atom ratio of Cu/Se is close to 1.89:1, indicating that the composition of the as-synthesized products is non-stoichiometric $Cu_{2-x}Se$.

The morphologies of the as-synthesized nanosheets were further investigated by TEM studies as shown in Fig. 4a, which also shows ultrathin micrometre-scale nanosheets. The SAED pattern shown in Fig. 4b taken along 20 irregularly ordered nanosheets shows several sharp rings, which could be indexed to the (111), (200), (220), (311), and (400) planes of the cubic crystalline structure of berzelianite. High-resolution TEM studies (Fig. 4d) confirm that typical lattice spacings are both ~0.333 and 0.288 nm, respectively, corresponding to (111) and (200) plane spacing of cubic phase $Cu_{2-x}Se$. The corresponding indexed fast Fourier transforms (FFTs, see Fig. 4c) of the lattice-resolved image can be indexed to the cubic structure of $Cu_{2-x}Se$ with the zone axes along the direction of (011), indicating that the nanosheets are well-crystallized, single crystalline in nature, and free from dislocation and stacking faults. Fig. 4e illustrates a schematic structure of the berzelianite lattice projected along the [011] orientation.

As shown in Fig. 1, single crystal cubic berzelianite nanoplates (in-plane diameter-to-thickness ratio ~10) were obtained with lower precursor Cu-to-Se ratio compared to that of the nanosheets. Fig. 5a and Figure S2 (see ESI†) show the SEM images of the product containing a large quantity of plate-like materials. Fig. 5b shows the high magnification SEM image of the nanoplates indicating that the size and morphology of the product is quite uniform. Figs. 5c, 5e, and 5f show several typical regularly-shaped (triangular, truncated triangular, and hexagonal) nanoplates with their basal planes parallel to the silicon substrate, revealing the in-plane diameters of the nanoplates as being between 200–300 nm. Fig. 5d shows several typical nanoplates with their basal planes oriented perpendicular to the silicon substrate, revealing the thickness of the nanoplates as being in the 20–30 nm range. As revealed by the distribution histograms (see ESI†), the in-plane diameter-to-thickness ratio is calculated

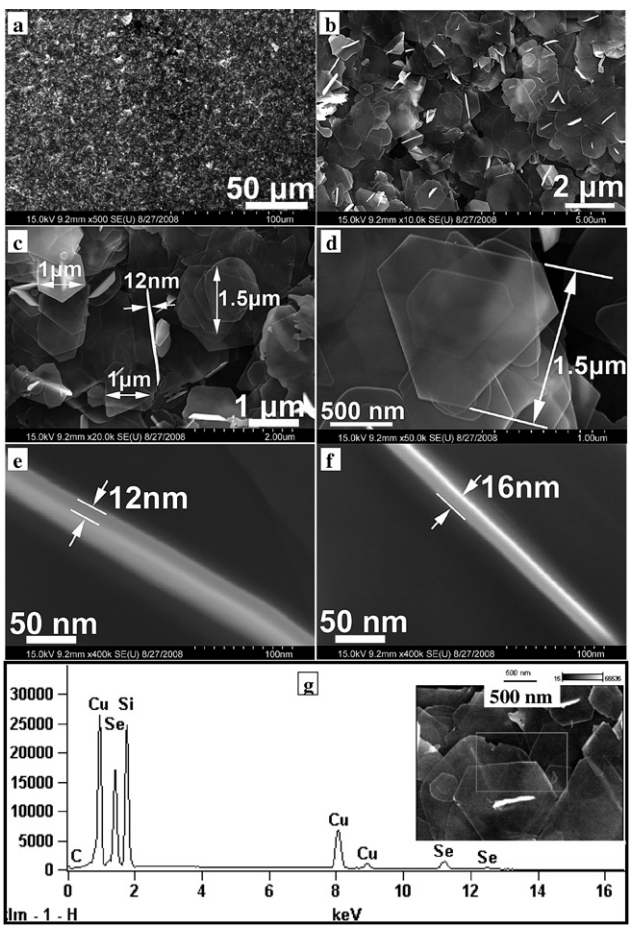

Fig. 3 (a–c) SEM images showing that the sample contains a large quantity of berzelianite nanosheets with in-plane diameter up to micrometre; (d) SEM image of a typical truncated triangular nanoplates with in-plane diameter of 1.5 μm; (e–f) enlarged SEM images showing that the thickness of typical nanosheets are only 12 and 16 nm, respectively; (g) EDS spectrum showing the possible composition of the nanosheets inset.

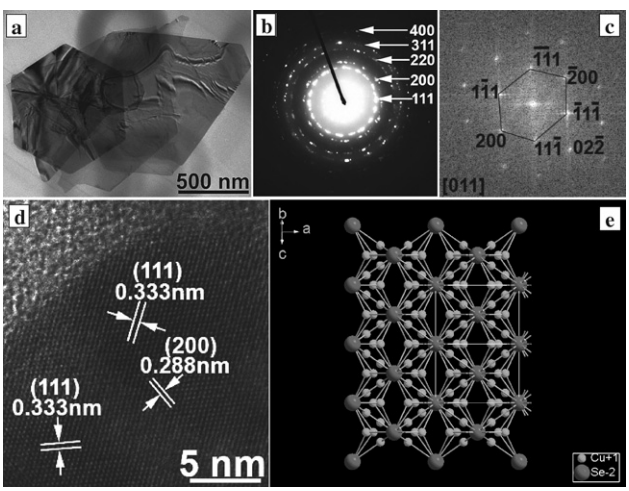

Fig. 4 (a) TEM image shows several ultrathin berzelianite nanosheets; (b) SAED spectrum of around 20 random oriented nanosheets; (d) HRTEM image and (c) its indexed fast Fourier transforms (FFTs) of the nanosheets; (e) The structure model of the berzelianite lattice projected along the [011] orientation. Structural features: close-packed Se layers in *c* stacking, Cu in tetrahedral and trigonal voids.

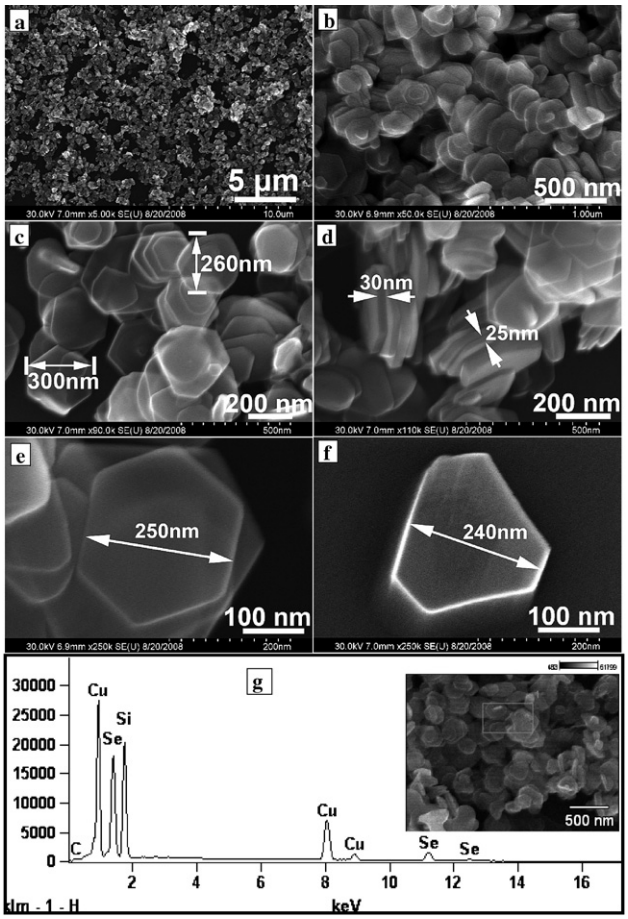

Fig. 5 (a–b) SEM images showing that the sample contains a large quantity of berzelianite nanoplates; (c) enlarged SEM image showing the typical in-plane diameter of the nanoplates are 240–300 nm; (d) enlarged SEM image showing the typical thickness of nanoplates are 25–30 nm; (e) SEM image of a typical hexagonal nanoplates with in-plane diameter of 250 nm; (f) SEM image of a typical truncated triangular nanoplates with in-plane diameter of 240 nm; (g) EDS spectrum showing the possible composition of the nanoplates inset.

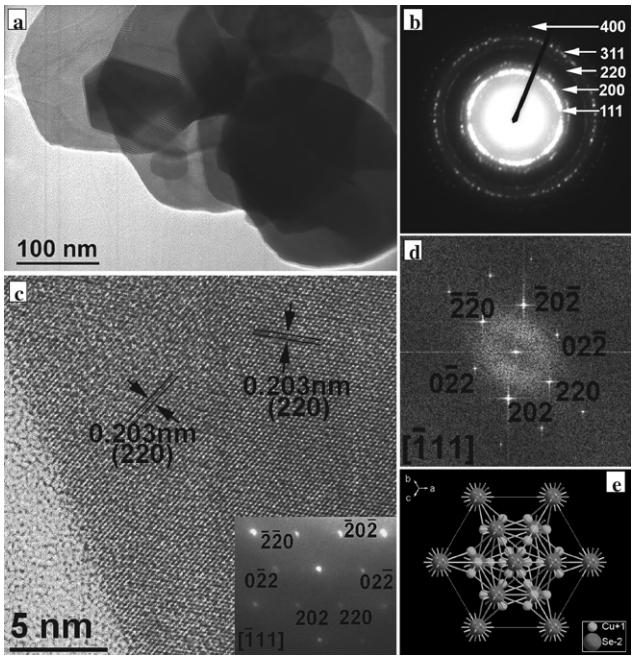

Fig. 6 (a) TEM image shows several berzelianite nanoplates; (b) SAED spectrum of around 20 randomly oriented nanoplates; (c) HRTEM image, (inset) SAED pattern, and (d) its indexed fast Fourier transforms (FFTs) of the nanoplates; (e) The structure model of the berzelianite lattice projected along the [111] orientation.

to be ~10. Fig. 5g is an EDS spectrum obtained from the nanoplates shown in the inset of Fig. 5g. Only Cu and Se peaks are observed (the silicon signal is from the substrate), suggesting that the nanoplates are composed mainly of Cu and Se. Quantitative EDS analysis shows that the atom ratio of Cu/Se is 1.85, indicating that the composition of the as-synthesized product is non-stoichiometric berzelianite.

The morphologies of the berzelianite nanoplates were investigated by TEM studies shown in Fig. 6a, which also shows the formation of nanoplates. The SAED pattern in Fig. 6b taken along 20 irregularly ordered nanoplates shows several obvious rings, which were indexed to the (111), (200), (220), (311), and (400) planes of the cubic crystalline structure of berzelianite. High-resolution TEM studies (Fig. 6c) confirm that typical lattice spacings are about 0.203 nm, corresponding to (220) plane spacing of the cubic phase berzelianite. The corresponding SAED pattern (inset to Fig. 6c) and the indexed FFTs of the lattice-resolved image (Fig. 6d) can be indexed to the cubic structure of berzelianite with the zone axes along the direction of (111), which is consistent with the schematic structure of berzelianite lattice projected along the [111] shown in Fig. 6e. All these results reveal that the as-synthesized nanoplates are well-crystallized, single crystalline in nature, and free from dislocation and stacking faults.

We now briefly discuss possible growth mechanisms of the nanosheets and nanoplates formed in paraffin liquid in the present study. Generally, for the synthesis of nanosheets and nanoplates, it was revealed that spherical nanoparticles were formed initially, followed by an aggregation of these small particles into a quasi-triangular or -hexagonal shape and the subsequent formation of crystalline nanosheets and nanoplates.[31] There generally exist two concepts in particle growth: Ostwald ripening mechanism[32] *vs.* oriented attachment mechanism,[33] *i.e.*, atom-by-atom addition growth *vs.* particle-by-particle growth. Oriented attachment involves spontaneous self-organization of adjacent particles, so that they share a common crystallographic orientation, followed by joining of these particles at a planar interface. Bonding between the nanocryatals reduces overall energy by removing surface energy associated with the nanocrystal-ligand interfaces.[33] In our experiments, berzelianite nuclei formed in the initial stage and further grew into nanocrystals. Then, nanocrystals were aggregated without sharing the same lattice plane. During the oriented attachment process, the adjacent aggregated nanocrystals are rotated to share a common crystallographic orientation to form bigger crystals, thus increasing the in-plane diameter. As shown in Figure S3 (see ESI†), the HRTEM image and its corresponding FFTs of the middle product in the formation of the nanosheet products harvested at the 250 °C after 3 min reaction time, show the

obvious "oriented attachment" growth process. Finally, single-crystal two-dimensional nanosheets and nanoplates are formed.

The exact role of changing the concentration of copper precursor in the controlling the formation of $Cu_{2-x}Se$ nanosheets and nanoplates is not yet to be completely understood. Considering the crystal growth in liquid medium, although the crystal growth habit is mainly determined by the intrinsic structure, it is also affected by the external conditions such as the temperature, ligands, and so on. Ligands such as EHA and OAm have different acid- and amine- functional groups, which have different oxopholicity when binding on the surface of the nanocrystals, leads to the production of anisotropic nanosheets and nanoplates. We believe that the major function of EHA and OAm was to prevent the nanoparticles from growing too large or aggregating into large entities in the nucleation stage. The in-plane diameter of $Cu_{2-x}Se$ nanostructures in the final product, as well as their thickness during the reaction, was found to strongly depend on the molar ratio between the ligand and copper precursor. Keeping the contraction of the ligands as a constant, when the copper precursor concentration was high (0.50 mmol), the in-plane diameter of the product could approach 1.0–2.5 μm. However, if the copper concentration was low (0.25 mmol), the in-plane diameter of the product in the final product would drop to 240–300 nm. We suppose that the ligand molecules could interact more strongly with some specific facets. In the present study, a relatively low copper concentration would probably heavily passivate the facets of product, resulting in small in-plane diameter. In a somewhat similar fashion to the micrometre-scale ultrathin berzelianite nanosheets with a cubic phase, our group has recently reported the synthesis of micrometre-scale ultrathin Ag nanosheets also with a cubic phase in a mixture solution of hexane and OAm.[34]

Our synthetic method is modular, and we have extended it to the synthesis of hexagal α-CuSe two-dimensional nanostructures by simply substituting the copper (I) chloride (CuCl) precursor with the copper (II) nitrate [$Cu(NO_3)_2$] as depicted in Figure S4 and Figure S5 (see ESI†). The exact in-plane diameter-to-thickness ratio of the α-CuSe product is different from that of $Cu_{2-x}Se$, possibly due to the difference in their intrinsic crystal structures (hexagonal klockmannite *vs.* cubic berzelianite). Besides the controllable synthesis of nanosheets and nanoplates with different in-plane diameter-to-thickness ratios achieved in the current study, it is expected that the morphologies and sizes of the products could be further tuned by changing the reaction parameters such as the reaction temperature and the concentration of the precursors and ligands.

Berzelianite is a well-known p-type semiconductor possessing a direct band gap as well as an indirect band gap; its band gap energy varies with the change of stoichiometry and phase. In order to understand the excitonic or interband transitions of the as-synthesized berzelianite nanosheets and nanoplates, UV-Vis-NIR absorption spectroscopy was performed on the samples. The results shown in Fig. 7a can be used to determine the band gap energies of the nanosheet and nanoplate products. As a crystalline semiconductor of indirect transition, the optical absorption near the band edge follows the formula: $\alpha h\nu = A(h\nu - E_g)^2$, where α, ν, and E_g are the absorption coefficient, optical frequency, and band gap energy, respectively, while A is a constant.[35] The band gap energy (E_g) can thus be estimated

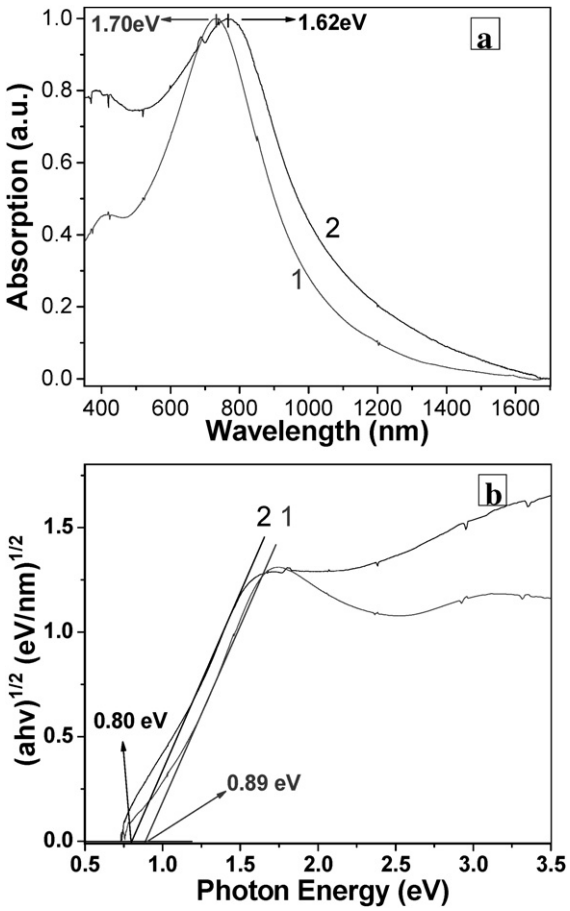

Fig. 7 (a) UV-Vis-NIR absorption spectra of the berzelianite nanosheets (line 1) and nanoplates (line 2) measured at room temperature; (b) the corresponding $(\alpha h\nu)^{1/2}$ *vs* photon energy ($h\nu$) plots of same spectra indicating their optical band gap energies are 0.80 eV and 0.89 eV, respectively.

from a plot of $(\alpha h\nu)^{1/2}$ *versus* the photon energy ($h\nu$), as shown in Fig. 7b. Using this method, indirect band gaps of about 0.89 and 0.80 eV, and intense optical absorption peaks at 1.70 eV and 1.62 eV, covering the entire red range of the solar spectrum, were obtained for berzelianite nanosheets and nanoplates. These values are closed to the reported band gap of 1.0–1.4 eV of the bulk berzelianite Cu_2Se, $Cu_{2-x}Se$, and klockmannite CuSe.[15] The estimated band gaps for nanosheets and nanoplates are very close to the optimum value for solar cell applications. The two-dimensional berzelianite nanostructures and nanoplates produced by the method in the present paper have potential applications in solar energy conversion as well as in a wide range of nano-photonic devices that operate in the red and near-infrared range of wavelengths.

4. Conclusions

A simple, low-cost, and environmentally-benign while effective colloidal chemical method was demonstrated for the first synthesis of two-dimensional single-crystal nanosheets (in-plane diameter-to-thickness ratio ~100) and nanoplates (in-plane diameter-to-thickness ratio ~10) of non-stoichiometric cubic

berzelianite. UV-Vis-NIR absorption spectroscopy reveals that the nanosheets and nanoplates have absorption onsets at 0.89 eV and 0.80 eV, respectively, and have intense optical absorption peaks at 1.70 eV and 1.62 eV, covering the entire red range of the solar spectrum. The present study expands the availability of two-dimensional nanostructures to binary chalcogenide semiconductor systems, while opening a new avenue to "green", low-cost synthesis of nanostructures with technological applications in solar energy conversion and also in a wide range of nanophotonic devices operating in the near-infrared. The feasibility of using paraffin liquid and simple organic acid and amine for controlled fabrication of two-dimensional berzelianite nanostructures may open a versatile route to other metal chalcogenide nanostructures as well.

Acknowledgements

We are grateful to Mr Philip Anderson and Prof. Supapan Seraphin at the University Spectroscopy & Imaging Facilities (USIF), the University of Arizona for help with the XRD and HRTEM characterizations. This work was supported by Science Foundation Arizona (Strategic Research Group Program).

References

1 W. U. Huynh, J. J. Dittmer and A. P. Alivisatos, *Science*, 2002, **295**, 2425.
2 I. Gur, N. Fromer, M. L. A. Geier and A. P. Alivisatos, *Science*, 2005, **310**, 462.
3 B. Tian, X. Zheng, T. J. Kempa, Y. Fang, N. Yu, G. Yu, J. Huang and C. M. Lieber, *Nature*, 2007, **449**, 885.
4 M. Law, L. E. Greene, J. C. Johnson, R. Saykally and P. D. Yang, *Nat. Mater.*, 2005, **4**, 455.
5 K. S. Leschkies, R. Divakar, J. Basu, E. Enache-Pommer, J. E. Boercker, C. B. Carter, U. R. Kortshagen, D. J. Norris and E. S. Aydil, *Nano Lett.*, 2007, **7**, 1793.
6 S. M. Sze, and K. K. Ng, *Physics of Semiconductor Devices*, 3rd Ed, Wiley, Hoboken, 2007.
7 Y. Yin and A. P. Alivisatos, *Nature*, 2005, **437**, 664.
8 A. Jennifer, B. L. S. M. Dahl and E. H. James, *Chem. Rev.*, 2007, **107**, 2228.
9 S. K. Haram, K. S. V. Santhanam, M. Numann-Spallar and C. Levy-Clement, *Mater. Res. Soc. Bull.*, 1992, **27**, 1185.
10 S. T. Lakshmikvmar, *Sol. Energy Mater. Sol. Cells*, 1994, **32**, 7.
11 G. Liu, T. Schulmeyer, J. Brötz, A. Klein and W. Jaegermann, *Thin Solid Films*, 2003, **431–432**, 477.
12 A. A. Korzhuev and F. Khim, *Obrab. Mater.*, 1991, **3**, 131.
13 W. S. Chen, J. M. Stewart and R. A. Mickelsen, *Appl. Phys. Lett.*, 1985, **46**, 1095.
14 V. Milman, *Acta Cryst.*, 2002, **B58**, 437.
15 O. Madelung, M. Schulz, and H. Weiss, *Landolt-Börnstein - Group III Condensed Matter Numerical Data and Functional Relationships in Science and Technology*. Springer-Verlag: Berlin, 1998 Vol. III/17E-17F-41C.
16 Y. Zhang, Z. P. Qiao and X. M. Chen, *J. Mater. Chem.*, 2002, **12**, 2747.
17 H. L. Li, Y. C. Zhu, S. Avivi, O. Palchik, J. P. Xiong, Y. Koltypin, V. Palchik and A. Gedanken, *J. Mater. Chem.*, 2002, **12**, 3723.
18 V. M. Glazov, A. S. Pashinkin and V. A. Fedorov, *Inorg. Mater.*, 2000, **36**, 641.
19 W. Wang, P. Yan, F. Liu, Y. Xie, Y. Geng and Y. Qian, *J. Mater. Chem*, 1998, **8**, 2321.
20 H. Lee, S. W. Yoon, E. J. Kim and J. Park, *Nano Lett.*, 2007, **7**, 778.
21 Y. Wu, C. Wadia, W. L. Ma, B. Sadtler and A. P. Alivisatos, *Nano Lett.*, 2008, **8**, 2551.
22 M. A. Malik, P. O'Brien and N. Revaprasadu, *Adv. Mater.*, 1999, **11**, 1441.
23 Y. Xie, X. W. Zheng, X. C. Jiang, J. Lu and L. Y. Zhu, *Inorg. Chem.*, 2002, **41**, 387.
24 Y. J. Hsu, C. M. Hung, Y. F. Lin, B. J. Liaw, T. S. Lobana, S. Y. Lu and C. W. Liu, *Chem. Mater.*, 2006, **18**, 3323.
25 S. Y. Zhang, C. X. Fang, Y. P. Tian, K. R. Zhu, B. K. Jin, Y. H. Shen and J. X. Yang, *Cryst. Growth Des.*, 2006, **6**, 2809.
26 X. B. Cao, C. Zhao, X. M. Lan, G. J. Gao, W. H. Qian and Y. Guo, *J. Phys. Chem. C*, 2007, **111**, 6658.
27 X. W. Zheng and Q. T. Hu, *Appl. Phys. A*, 2009, **94**, 805.
28 Z. T. Deng, L. Cao, F. Q. Tang and B. S. Zou, *J. Phys. Chem. B*, 2005, **109**, 16671.
29 J. A. Dahl, B. L. S. Maddux and J. E. Hutchison, *Chem. Rev.*, 2007, **107**, 2228.
30 Z. T. Deng, M. Mansuripur and A. J. Muscat, *Nano Lett.*, 2009, **9**, 2015.
31 W. L. Huang, C. H. Chen and M. H. Huang, *J. Phys. Chem. C*, 2007, **111**, 2533.
32 E. Matijevic, *Annu. Rev. Mater. Sci.*, 1985, **15**, 483.
33 R. L. Penn and J. F. Banfield, *Science*, 1998, **281**, 969.
34 Z. T. Deng, M. Mansuripur and A. J. Muscat, *J. Phys. Chem. C*, 2009, **113**, 867.
35 Z. T. Deng, D. Chen, B. Peng and F. Q. Tang, *Cryst. Growth Des.*, 2008, **8**, 2995.

